YIELD ESTIMATION FROM HYPERSPECTRAL IMAGERY USING SPECTRAL ANGLE MAPPER (SAM)

C. Yang, J. H. Everitt, J. M. Bradford

ABSTRACT. *Vegetation indices (VIs) derived from remotely sensed imagery are commonly used to estimate crop yields. Spectral angle mapper (SAM) provides an alternative approach to quantifying the spectral differences among all pixels in an image and therefore has the potential for mapping yield variability. The objective of this study was to apply the SAM technique to airborne hyperspectral imagery for mapping yield variability. Airborne hyperspectral imagery was acquired from two grain sorghum fields in south Texas, and yield data were collected using a grain yield monitor. SAM images were generated from the hyperspectral images based on six reference spectra extracted directly from the hyperspectral images and four reflectance spectra measured on the ground. Statistical analysis showed that the ten SAM images for each field produced similar correlation coefficients with yield. For comparison, all 5151 possible narrow-band normalized difference vegetation indices (NDVIs) were derived from the 102-band images and related to yield. Results showed that the SAM images based on the soil reference spectra provided higher correlation coefficients with yield than 75% and 92% of the 5151 narrow-band NDVIs for fields 1 and 2, respectively. Like an NDVI image, a SAM image can be easily generated from a hyperspectral image to characterize the spatial variability in yield. Moreover, since the best NDVI typically varies with yield datasets, a SAM image based on a single reference spectrum can be a better representation of yield variability if actual yield data are not available for the identification of the best NDVI. The results from this study indicate that the SAM technique can be used alone or in conjunction with other VIs for yield estimation from hyperspectral imagery.*

Keywords. *Hyperspectral imagery, Normalized difference vegetation index (NDVI), Remote sensing, Spectral angle mapper (SAM), Yield estimation, Yield monitor.*

Vegetation indices (VIs) derived from the spectral bands in multispectral imagery have commonly been used for crop yield estimation (Wiegand et al., 1991; Senay et al., 1998; GopalaPillai and Tian, 1999; Plant et al., 2000; Yang and Everitt, 2002). These VIs are usually formed from combinations of visible and near-infrared (NIR) wavebands. Two of the earliest and most widely used VIs are the simple ratio (NR = NIR/Red) (Jordan, 1969) and the normalized difference vegetation index [NDVI = (NIR - Red)/(NIR + Red)] (Rouse et al., 1973). Others include band ratios (BN = Blue/NIR and GN = Green/NIR) and normalized differences such as the blue NDVI [BNDVI = (NIR - Blue)/(NIR + Blue)] and the green NDVI [GNDVI = (NIR - Green)/(NIR + Green)]. Yang and Everitt (2002) used band ratios NR and NG as well as normalized differences NDVI and GNDVI derived from airborne color-infrared (CIR) imagery to generate yield maps for delineating within-field spatial variability as compared with yield monitor data.

In recent years, airborne hyperspectral imagery has been evaluated for yield estimation (Goel et al., 2003; Yang et al., 2004a, 2004b; Jang et al., 2005). Hyperspectral imagery contains tens to hundreds of narrow spectral bands. These nearly continuous spectral data have the potential for better differentiation and estimation of biophysical attributes of interest. Thenkabail et al. (2000) related crop variables to ground reflectance data measured in 490 discrete narrow bands between 350 and 1,050 nm to identify the optimum bands using multiple regression analysis. They also calculated narrow-band NDVIs involving all possible two-band combinations of 490 bands and identified the best narrow-band NDVIs for each crop variable. Yang et al. (2004a) applied stepwise regression analysis on grain sorghum yield monitor data and 102-band airborne hyperspectral imagery to identify optimum band combinations for mapping yield variability. They also used principal components analysis (PCA) and stepwise regression to select the significant principal components to account for the yield variability. To demonstrate the advantage of narrow hyperspectral bands over broad multispectral bands for yield estimation, Yang et al. (2004b) aggregated hyperspectral bands into the Landsat-7 ETM+ sensor's four broad visible and NIR bands and found that the combinations of significant narrow bands explained more yield variability than the four broad bands.

Although multiple regression and narrow-band NDVI analysis can be used to identify the optimum bands for yield estimation, these bands are only the best for the particular

Submitted for review in February 2007 as manuscript number IET 6894; approved for publication by the Information & Electrical Technologies Division of ASABE in March 2008. Presented at the 2006 ASABE Annual Meeting as Paper No. 061168.

Mention of trade names or commercial products in this article is solely for the purpose of providing specific information and does not imply recommendation or endorsement by the USDA.

The authors are **Chenghai Yang, ASABE Member,** Agricultural Engineer, **James H. Everitt,** Range Scientist, and **Joe M. Bradford,** Supervisory Soil Scientist, USDA-ARS Kika de la Garza Subtropical Agricultural Research Center, Weslaco, Texas. **Corresponding author:** Chenghai Yang, USDA-ARS Kika de la Garza Subtropical Agricultural Research Center, 2413 E. Highway 83, Weslaco, TX 78596; phone: 956-969-4812; fax: 956-969-4800; e-mail: chenghai.yang@ ars.usda.gov.

image and yield data set from which they are derived and may not be the best for a different data set. For example, Yang et al. (2004a) identified four optimum bands using stepwise regression for one field and seven completely different bands for a second field for estimating grain sorghum yield. Similarly, the optimum NDVI identified for one data set may not be the best for another. Moreover, the number of narrow-band NDVIs for a hyperspectral image can be so large that it may not be practical to find the optimum NDVI for each data set. For example, there are a total of 128!/(126! × 2!) = 8128 possible narrow-band NDVI images for a 128-band hyperspectral image. Therefore, it is necessary to use a technique that takes advantage of the spectral information in all the bands and still provides a good estimate of yield.

Spectral angle mapper (SAM) is a spectral technique that measures the similarity of image pixel spectra to reference spectra (Kruse et al., 1993). The reference spectra can be either laboratory or field spectra, or spectra extracted from the image for the known ground materials. The ground materials are often referred to as endmembers and their spectra as endmember spectra. SAM measures similarity by calculating the angle between an image pixel spectrum and a reference spectrum, treating them as vectors in a space with dimensionality equal to the number of bands (Kruse et al., 1993).

A multispectral or hyperspectral image can be viewed as a collection of band images, and each image pixel contains a spectrum of reflectance values for all the wavebands in the image. If a material such as healthy crop plants or bare soil occupies the whole pixel, then the pixel spectrum may be considered as the endmember spectrum of the ground material. For each endmember chosen, a spectral angle is determined for every pixel in the image, and this angle value is assigned to that pixel in the output spectral angle map or SAM image. Smaller angle values indicate higher similarity between the pixel and the endmember. The number of derived SAM images is equal to the number of endmember spectra used in the mapping. The spectral angle is insensitive to gain factors (such as solar illumination) since the angle between two vectors is independent of their length.

SAM has been used as a supervised classification method for a variety of hyperspectral remote sensing applications (Crósta et al., 1998; Rowan and Mars, 2003; Dennison et al., 2004; Clark et al., 2005; Mundt et al., 2005). However, there is no report on the use of SAM for mapping crop yield. Like VIs, the spectral angle is an indirect measure of plant vigor and abundance when applied in vegetation mapping. When the endmember is a healthy crop canopy, small angle values correspond to high-vigor plants and large values correspond to low-vigor plants. On the other hand, if the endmember is bare soil, then small values may indicate low-vigor plants and large values may indicate high-vigor plants. Therefore, the spectral angle can be used as a VI to estimate crop canopy abundance and thus crop yield.

The objectives of this study were to (1) apply SAM to airborne hyperspectral imagery for mapping grain sorghum yield variability, and (2) relate grain yield monitor data with SAM images and compare the results with those for all possible narrow-band NDVIs derived from the hyperspectral imagey.

Methods

Imagery and Yield Data Collection and Preprocessing

Two irrigated grain sorghum fields, owned and managed by Rio Farms, Inc., at Monte Alto, Texas, were selected for this study. These fields were 19 ha and 14 ha in size and designated as fields 1 and 2, respectively. The geographic coordinates near the centers of fields 1 and 2 were (98° 00′ 05″ W, 26° 29′ 28″ N) and (98° 02′ 28″ W, 26° 28′ 55″ N), respectively. The soil is Hidalgo fine sandy loam in field 1 and Rio fine sandy loam in field 2. Grain sorghum and cotton are normally grown in rotation in these fields. Grain sorghum (AgriPro 9850) was planted to the two fields in late February and harvested in late June in 2000.

A hyperspectral imaging system described by Yang et al. (2003) was used to acquire images from the fields. The system consisted of a digital CCD camera, a prism-grating-prism hyperspectral filter, a front lens, and a PC equipped with a frame grabbing board and camera utility software. For this study, the hyperspectral system was configured to capture imagery with 128 bands covering a spectral range from 457.2 to 921.7 nm at 3.63 nm intervals. The imagery had a swath width of 640 pixels and a radiometric resolution of 12 bits.

A Cessna 206 single-engine aircraft was used as the platform for image acquisition. The hyperspectral imaging system was mounted on a light aluminum frame along with a three-camera multispectral imaging system described by Escobar et al. (1997). The three-camera system was used as a viewfinder to locate the target since the hyperspectral system did not provide an overall view of the imaging area. No stabilizer or inertial measurement device (IMU) was used to dampen or measure platform variations, but care was taken to minimize the effects of winds and changes in the aircraft's speed and flight direction. For the given number of bands to be captured and the sizes of the fields to be imaged, a flight height of 1680 m (5500 ft) above ground level and a flight speed of 150 km/h (93 mi/h) were predetermined. The aircraft was stabilized at the predetermined flight altitude, speed, and direction before the start of image acquisition and was maintained at the same altitude, speed, and direction during the course of image acquisition. Hyperspectral images were acquired under sunny and calm conditions from the two grain sorghum fields on 27 April 2000 after the crop achieved its maximum canopy cover. The swath of the imagery was approximately 840 m and the ground pixel size achieved was 1.3 m.

The geometric distortions in the imagery due to the variations of the platform were corrected using a reference line approach described by Yang et al. (2003). A reference line, such as a straight field boundary or a road within the image area, approximately parallel to the flight line was first identified and the corresponding distorted line on the raw image was manually digitized. Then the shift in pixels between the reference line and the distorted line was determined for each row of the raw image. Finally, each row was shifted in the across-track direction by the number of pixels determined.

The geometrically restored hyperspectral images for the two fields were rectified based on their respective photographic images, which were taken in the growing season and georeferenced to the Universal Transverse Mer–

cator (UTM), World Geodetic Survey 1984 (WGS-84), Zone 14, coordinate system. The images were resampled to 1 m pixel resolution using the nearest-neighbor algorithm during the rectification process. The root mean square (RMS) errors for the rectified hyperspectral images were 3.8 and 4.3 m for fields 1 and 2, respectively, based on first-order polynomial transformations. The relatively high RMS errors were mainly due to other geometric distortions not corrected by the reference line method.

For radiometric calibration, three 8 × 8 m tarpaulins with reflectance values of 4%, 32%, and 48%, respectively, were placed near the fields during image acquisition. The reflectance values from the tarpaulins were measured using a FieldSpec HandHeld spectroradiometer (Analytical Spectral Devices, Inc., Boulder, Colo.) sensitive in the 350 to 1,050 nm portion of the spectrum with a spectral sampling interval of 1.4 nm. The instrument was also used to take reflectance spectra from grain sorghum plants, bare soil, and highway surface in the imaging areas. The rectified hyperspectral images were converted to reflectance based on 128 calibration equations (one for each band) relating reflectance values to the digital count values extracted from the three tarpaulins on the images. All procedures for image rectification and calibration were performed using ERDAS IMAGINE (Leica Geosystems Geospatial Imaging, LLC, Norcross, Ga.). Because the camera had low quantum efficiency near the NIR end of the observed spectrum, the reflectance values for wavelengths greater than 846 nm were not reliable. In addition, the first few bands in the blue region appeared to be noisy. Therefore, bands 1-5 and 108-128 (a total of 26 bands) were removed from each hyperspectral image, and the remaining 102 bands with center wavelengths from 477.2 to 843.7 nm were used for analysis.

Yield data were collected using an Ag Leader Yield Monitor 2000 system (Ag Leader Technology, Ames, Iowa). Instantaneous yield, moisture, and GPS data were simultaneously recorded at 1 s intervals. The yield monitor was calibrated to ensure data accuracy before grain was harvested. The combine equipped with the yield monitoring system had an effective cutting width of 8.69 m. The yield and GPS data from the yield monitor were viewed, cleaned, and then exported in ASCII format using SMS Basic software (Ag Leader Technology, Ames, Iowa). An optimum time lag of 14 s, as determined with the method of Yang et al. (2002), was used to align yield with position data, and the yield data were adjusted to 14% moisture content.

SAM Analysis

The angle of the two spectra is calculated by the following formula (Kruse et al., 1993):

$$\alpha = \cos^{-1}\frac{\mathrm{X}\cdot\mathrm{R}}{|\mathrm{X}||\mathrm{R}|} = \cos^{-1}\frac{\sum_{i=1}^{n} x_i r_i}{\sqrt{\sum_{i=1}^{n} x_i^2}\sqrt{\sum_{i=1}^{n} r_i^2}} \qquad (1)$$

where X is an image pixel spectrum, R is a reference spectrum or an endmember spectrum, α is the spectral angle between X and R measured in radians or degrees, and n is the number of bands in the image.

The first step in SAM analysis is to determine the endmembers and their spectra. Endmember spectra can be obtained from the image, ground, or a spectral library. However, spectra derived directly from the image data are usually better than ground or library spectra because the image spectra more accurately account for any errors in calibration or atmospheric correction and sensor response effects. Because of different plant growth stages and temporally variant soil surface and moisture conditions during a growing season, the reflectance spectra of crop plants and soil background change from time to time. Therefore, it may be better to use the endmember spectra derived from an image only for that particular image. In this study, grain sorghum plants and bare soil were selected as two meaningful endmembers. To obtain pure spectra for sorghum plants, 50 pixels that had a bright red color (corresponding to healthy plants on a CIR image) were identified from each image. Similarly, 50 pixels that contained pure bare soil were identified from each image. These pixels were extracted from the areas with known healthy plants and bare soil on the ground. The endmember spectra for healthy plants and bare soil for each image were obtained by averaging the spectra of the respective pixels from that image.

In order to examine how the selection of endmembers affects the SAM results, spectra for highway surface and wet soil in the image for field 1 were extracted. Additionally, ground reflectance spectra taken for healthy grain sorghum plants, bare soil, highway surface, and water from or near field 2 at the time of image acquisition were also used as reference spectra. Thus, there were a total of six image reference spectra (two plant spectra, two dry soil spectra, one highway surface spectrum, and one wet soil spectrum) and four ground reference spectra. Although the ten spectra were from different images and ground surfaces, they were all used for the calculation of SAM images for each field. ENVI (Research Systems, Inc., Boulder, Colo.) was used for SAM analysis.

NDVI and Statistical Analysis

The 102-band hyperspectral image and the ten SAM images for each field were converted into grids in ArcInfo (ESRI, Inc., Redlands, Cal.). The preprocessed yield data were imported into ArcInfo as point coverages. Since the combine's effective cutting width was 8.69 m and the cell size of the image data was 1 m, these images were aggregated by a factor of 9 to increase the cell size to 9 m. The digital value for each output cell was the mean of the 81 input cells that the 9 m × 9 m output cell encompassed. The yield value for each output cell was the mean of the yield points falling within the 9 m × 9 m output cell. On the average, each output cell contained approximately five yield data points.

A total of 5151 [102!×(100!/2!)] narrow-band NDVIs were calculated from the 102 bands in each hyperspectral image. Correlation matrices were calculated among grain sorghum yield, the ten SAM images, and the 5151 NDVI images for each field. Linear regression was used to determine the best-fitting equations for relating yield to the SAM images and the best NDVIs. SAS software (SAS Institute, Inc., Cary, N.C.) was used for statistical analysis.

Results and Discussion

Figure 1 shows the reflectance spectra for healthy grain sorghum plants and dry bare soil extracted from the hyperspectral images for fields 1 and 2. The spectra for highway surface and wet soil extracted from the image for field 1 are also presented. Figure 2 shows the ground reflectance spectra for healthy sorghum plants, dry bare soil, highway surface, and water taken from or near field 2 at the time of image acquisition. The spectra extracted from the images were slightly noisy compared with the ground spectra. The three spectra for healthy plants had the typical shape for vegetation, but were slightly different in magnitude from one another because each spectrum represented the spectral response of a different plant canopy. The three spectra for dry bare soil were close to straight lines and very similar in magnitude. The two highway surface spectra also had a similar shape, but the spectrum taken on the ground had slightly higher reflectance because it was taken from a different spot on the highway from the area the image spectrum was extracted.

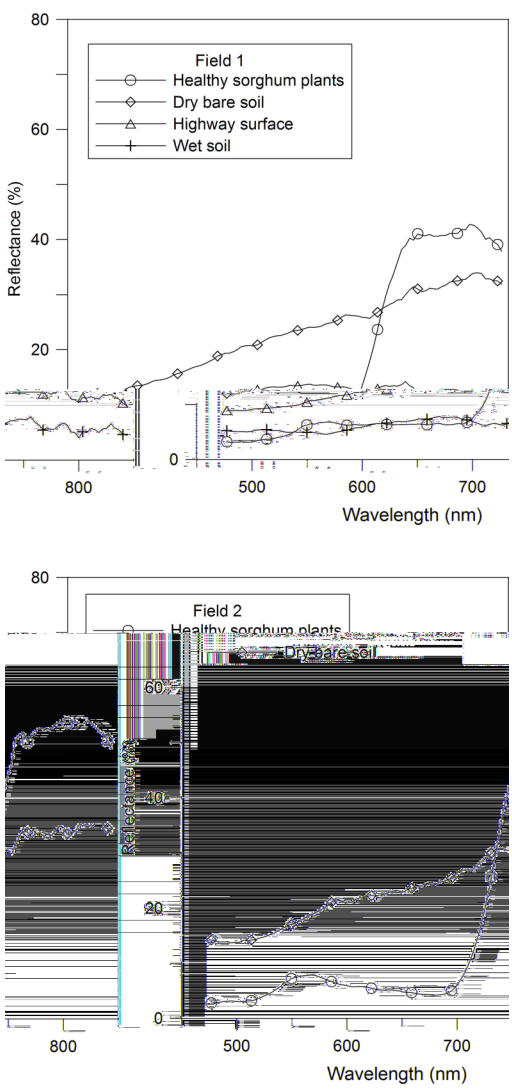

Figure 1. Reflectance spectra for healthy grain sorghum plants and dry bare soil derived from 102-band airborne hyperspectral images for fields 1 and 2. Spectra for highway surface and wet soil from the image for field 1 are also shown.

Table 1 presents the spectral angles among the ten reference spectra. Spectral angles ranged from 2.4° between the image dry soil spectrum from field 2 and the ground soil spectrum to 68.1° between the image plant spectrum from field 2 and the ground water spectrum. As expected, spectral angles between similar cover types were smaller than those between different cover types. For example, grain sorghum plants had spectral angles from 25° to 33° with dry bare soil, from 38° to 46° with highway surface, from 44° to 48° with wet bare soil, and from 65° to 68° with water. Clearly, grain sorghum plants had large spectral differences from dry soil, highway surface, wet soil, and water.

Table 2 summarizes the simple spectral angle statistics for the SAM images derived from the hyperspectral images for fields 1 and 2 based on the ten reference spectra. Mean spectral angles varied from 8.1° to 59.8° for field 1 and from 9.3° to 58.8° for field 2. However, the standard deviation values of the SAM images were similar among the ten endmembers for each field, indicating that the SAM images based on different reference spectra had similar variations in spectral angle.

Figures 3 and 4 show the SAM images based on the dry soil reference spectra extracted from the images for fields 1 and 2, respectively. Dark areas have small spectral angles and represent pixels with large soil exposure and sparse plant stands. Conversely, light areas have large spectral angles and represent pixels with healthy plants. The SAM images based on the reference spectra for highway surface, wet soil, and water have similar gray patterns to those based on the dry soil spectra. However, the SAM images based on the plant spectra had opposite patterns. Small spectral angles represent healthy plants, while large spectral angles indicate low-vigor plants and large soil exposure.

Table 3 shows the correlation coefficients between grain yield monitor data and the SAM images based on the ten reference spectra for both fields. Grain yield was significantly negatively related with the SAM data based on the plant spectra and positively related to the SAM data based on the other non-plant reference spectra. Although all the reference spectra had similar r-values, the ground water

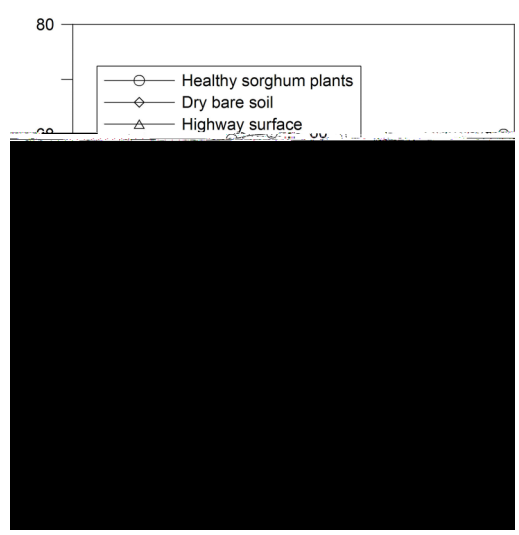

Figure 2. Ground reflectance spectra for healthy grain sorghum plants, dry bare soil, highway surface, and water taken from or near field 2 with a spectroradiometer.

Table 1. Spectral angles in degrees among ten endmember spectra (reference spectra) derived from 102-band airborne hyperspectral images and taken on the ground.

Endmember	Plant1	Plant2	Plant3	Soil1	Soil2	Soil3	Road1	Road3	Wetsoil1	Water3
Plant1[a]	0	5.2	3.9	24.5	29.2	29.4	42.1	38.3	44	65.3
Plant2[b]		0	4.4	28.7	33.2	33.4	46	42.2	47.9	68.1
Plant3[c]			0	26.2	30.8	30.9	43.6	39.6	45.6	65.9
Soil1				0	5.7	5.6	18.4	14.9	21.1	45.9
Soil2					0	2.4	14	10.3	17.1	41.9
Soil3						0	14.1	10.3	16.9	41.9
Road1							0	5.5	6.1	31.3
Road3								0	10.1	32.4
Wetsoil1									0	32.7
Water3										0

[a] Plant1, soil1, road1, and wetsoil1 = Spectra for healthy grain sorghum plants, dry bare soil, highway surface, and wet bare soil derived from a 102-band airborne hyperspectral image for field 1.
[b] Plant2 and soil2 = Spectra for healthy grain sorghum plants and bare soil derived from a 102-band airborne hyperspectral image for field 2.
[c] Plant3, soil3, road3, and water3 = Spectra for healthy grain sorghum plants, bare soil, highway surface, and water measured from or near field 2 with a spectroradiometer.

Table 2. Simple spectral angle statistics in degrees for ten SAM (spectral angle mapper) images derived from 102-band airborne hyperspectral images for fields 1 and 2 based on ten endmember spectra (reference spectra).

	Field 1				Field 2			
Endmember	Min	Mean	Max	STD	Min	Mean	Max	STD
Plant1[a]	3.5[b]	8.1	27.8	4.6	3.6	9.3	35	7.7
Plant2[c]	5.3	11.9	32	4.9	2.5	11.3	38.9	8.9
Plant3[d]	4.6	9.9	29.6	4.6	3.8	10.1	36.4	8.1
Soil1	3.3	18.2	26	5	5.2	19.6	28.1	6.1
Soil2	5.8	22.8	30.5	5.1	4	23.2	32.7	7.7
Soil3	5.4	23.1	30.8	5.1	4.4	23.5	32.9	7.7
Road1	16	35.6	43.4	5.2	8.9	35.5	45.4	8.9
Road3	12.8	31.9	39.6	5.1	4.3	31.5	41.6	9
Wetsoil1	18.5	37.7	45.3	5	12.7	37.7	47.4	8.6
Water3	43.9	59.8	66.1	4.3	35.1	58.8	67.6	7.8

[a] Plant1, soil1, road1, and wetsoil1 = Spectra for healthy grain sorghum plants, dry bare soil, highway surface, and wet bare soil derived from a 102-band airborne hyperspectral image for field 1.
[b] Number of samples (pixels) = 2265 for field 1 and 1658 for field 2.
[c] Plant2 and soil2 = Spectra for healthy grain sorghum plants and bare soil derived from a 102-band airborne hyperspectral image for field 2.
[d] Plant3, soil3, road3, and water3 = Spectra for healthy grain sorghum plants, bare soil, highway surface, and water measured from or near field 2 with a spectroradiometer.

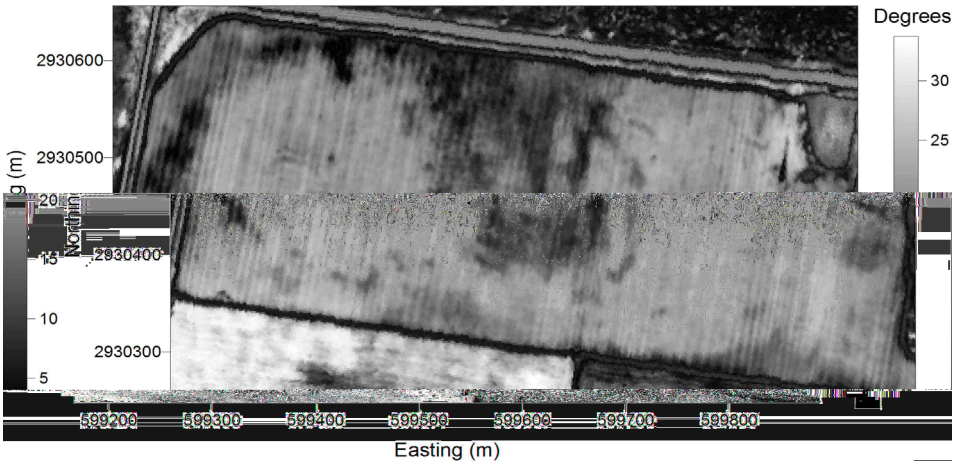

Figure 3. SAM (spectral angle mapper) image derived from a 102-band airborne hyperspectral image for field 1 based on a dry bare soil reference spectrum extracted from the image.

reference spectrum resulted in the highest r-value (0.782) for field 1, and the dry soil spectrum derived from field 2 and the ground soil spectrum produced the highest r-value (0.841) for field 2. Evidently, the three plant spectra had slightly lower r-values than the other reference spectra. This is because the plant reference spectra obtained from the images or on the ground may not represent the plants that had the highest yield. Although plant reference spectra corresponding to high yield can be generally accurately identified based on the CIR image, there is no guarantee that the identified spectra

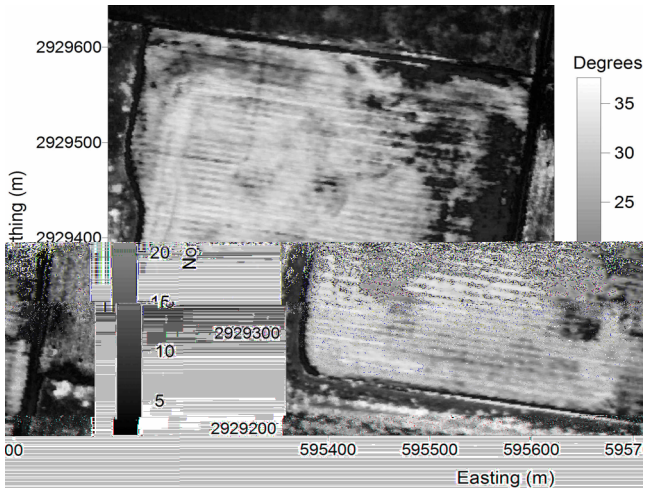

Figure 4. SAM (spectral angle mapper) image derived from a 102-band airborne hyperspectral image for field 2 based on a dry bare soil reference spectrum extracted from the image.

represent the healthy plants with highest yield. On the other hand, reference spectra derived from bare soil, highway surface, or water always represent the areas with zero yield. Therefore, it may be more reliable and accurate to use soil spectra as reference spectra for generating SAM images because bare soil can be found around any field. Moreover, image-derived reference spectra had essentially the same results as ground spectra for soil and highway surface.

Table 4 summarizes the univariate statistics of absolute correlation coefficients between grain yield and all 5151 NDVIs derived from the 102-band hyperspectral images for fields 1 and 2. The r-values varied from 0.000 to 0.811 for field 1 and from 0.001 to 0.879 for field 2. The center wavelengths that resulted in lowest r-values were 561 and 564 nm for field 1 and 778 and 822 nm for field 2, and the center wavelengths that resulted in highest r-values were 543 and 728 nm for field 1 and 742 and 789 nm for field 2. Clearly, the best NDVIs resulted in higher correlations with yield than the SAM images for both fields. Nevertheless, the SAM-based best r-values were better than the mean, median, or 75% quantile of the NDVI-based absolute r-values for each field. In fact, the SAM-based best r-values (0.782 and 0.841) were higher than 80% and 95% of the 5151 NDVI-based r-values for fields 1 and 2, respectively. In addition, the SAM images based on the soil reference spectra provided higher r-values with yield than at least 75% and 92% of the 5151 narrow-band NDVIs for fields 1 and 2, respectively. The higher r-values from the NDVI approach was at the cost of intensive calculations of all 5151 NDVI images, compared with only a few images based on the SAM approach. Therefore, if the goal is to derive a spectral map from a hyperspectral image to show the spatial variability in yield without knowing the actual yield, then a SAM image based on a reference spectrum will be a better choice. However, if the goal is to determine the best correlation based on the actual ground data, then all NDVIs can be derived to identify the best one. Current commercial image processing software has the capability to generate SAM images based on reference spectra, but it does not have the functionality to automatically calculate all possible NDVIs for hyperspectral imagery.

Figures 5 and 6 show contour maps of absolute r-values between yield and all possible NDVIs for fields 1 and 2, respectively. Since $NDVI_{ij} = 0$ when band i = band j, r-values do not exist on the diagonal line. Although it suffices to show the contour map below or above the diagonal line for each field, a square map is presented based on the symmetry of the absolute r-values for the 5151 band pairs. These contour maps clearly illustrate the r-value distributions for all the band pairs. For field 1, r-values were generally higher when one band had wavelengths below 720 nm and the other band had wavelengths above 720 nm than when both bands in a pair had wavelengths below 720 nm or above 750 nm. The contour map for field 2 has some similarities to and differences from the contour map for field 1. The r-values were also generally higher when one band had wavelengths below 720 nm and the other band had wavelengths above 720 nm than when both bands in a pair had wavelengths above 750 nm. Unlike for field 1, most of the r-values for band pairs with wavelengths above 540 nm and below 700 nm were generally high for field 2. Nevertheless, it is more likely to obtain better NDVI images by selecting one band

Table 3. Correlation coefficients between grain sorghum yield and ten SAM (spectral angle mapper) images derived from 102-band airborne hyperspectral images for fields 1 and 2 based on ten endmember spectra (reference spectra).

Endmember	Field 1	Field 2
Plant1[a]	-0.768[b]	-0.787
Plant2[c]	-0.767	-0.827
Plant3[d]	-0.759	-0.801
Soil1	0.772	0.836
Soil2	0.774	0.841
Soil3	0.772	0.841
Road1	0.772	0.831
Road3	0.774	0.830
Wetsoil1	0.772	0.832
Water3	0.782	0.830

[a] Plant1, soil1, road1, and wetsoil1 = Spectra for healthy grain sorghum plants, dry soil, highway surface, and wet soil derived from a 102-band airborne hyperspectral image for field 1.

[b] All r-values were significant at the $p < 0.0001$ level. Number of samples (pixels) = 2265 for field 1 and 1658 for field 2.

[c] Plant2 and soil2 = Spectra for healthy grain sorghum plants and dry soil derived from a 102-band airborne hyperspectral image for field 2.

[d] Plant3, soil3, road3, and water3 = Spectra for healthy grain sorghum plants, bare soil, highway surface, and water measured on the ground with a spectroradiometer.

Table 4. Univariate statistics of absolute correlation coefficients (r) between grain sorghum yield and all possible NDVIs derived from 102-band airborne hyperspectral images for fields 1 and 2.

Statistics[a]	Field 1	Field 2
Min[b]	0.000	0.001
25% Quantile	0.366	0.766
Mean	0.569	0.747
Median	0.724	0.821
75% Quantile	0.771	0.829
Max[c]	0.812	0.879

[a] The number of NDVIs was 5151. $NDVI_{ij} = (R_j - R_i)/(R_i + R_j)$, where R_i is the reflectance for band i, $i = 1, 2, ..., 101$ and $j = i + 1, ..., 102$. Correlation was significant at 0.0001 level if $r > 0.079$ for field 1 and if $r > 0.093$ for field 2. The number of samples (pixels) used to calculate each r-value was 2265 for field 1 and 1658 for field 2.

[b] Center wavelengths were 561 and 564 nm for field 1, and 778 and 822 nm for field 2.

[c] Center wavelengths were 543 and 728 nm for field 1, and 742 and 789 nm for field 2.

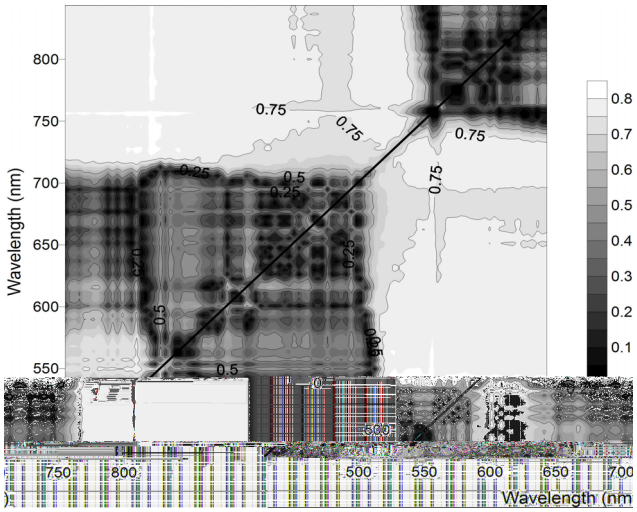

Figure 5. Contour map showing absolute correlation coefficients between grain sorghum yield and all possible narrow-band NDVIs derived from a 102-band airborne hyperspectral image for field 1. When band *i* = band *j*, $NDVI_{ij}$ = 0 and r values do not exist (shown by the diagonal line).

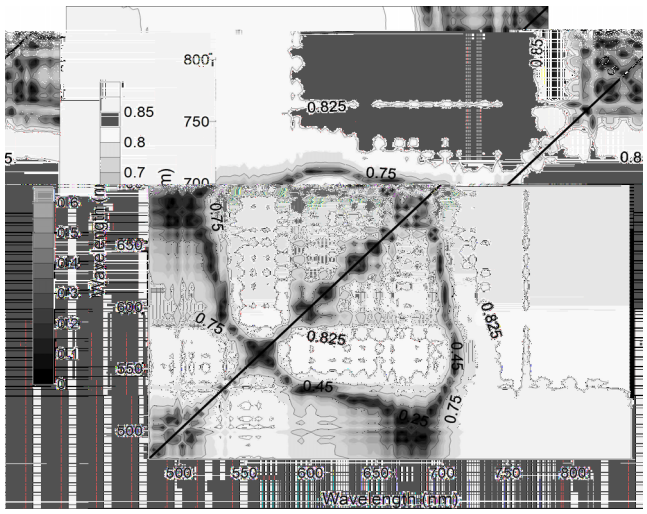

Figure 6. Contour map showing absolute correlation coefficients between grain sorghum yield and all possible narrow-band NDVIs derived from a 102-band airborne hyperspectral image for field 2. When band *i* = band *j*, $NDVI_{ij}$ = 0 and r values do not exist (shown by the diagonal line).

with wavelengths below 720 nm and the other above 720 nm for both fields.

Figures 7a and 8a show scatter plots and regression lines between grain yield and the SAM images based on the dry soil spectra extracted from the hyperspectral images for fields 1 and 2, respectively. For comparison, scatter plots and regression lines between grain yield and the best NDVIs for the respective fields are also presented in figures 7b and 8b. Although the SAM images provided better yield estimation than most of the NDVIs, the best NDVIs had better relations with yield. The SAM images based on the dry soil reference spectra explained 60% and 71% of the variability in yield for fields 1 and 2, respectively, while the best NDVIs explained 66% and 77% of the variability for the respective fields.

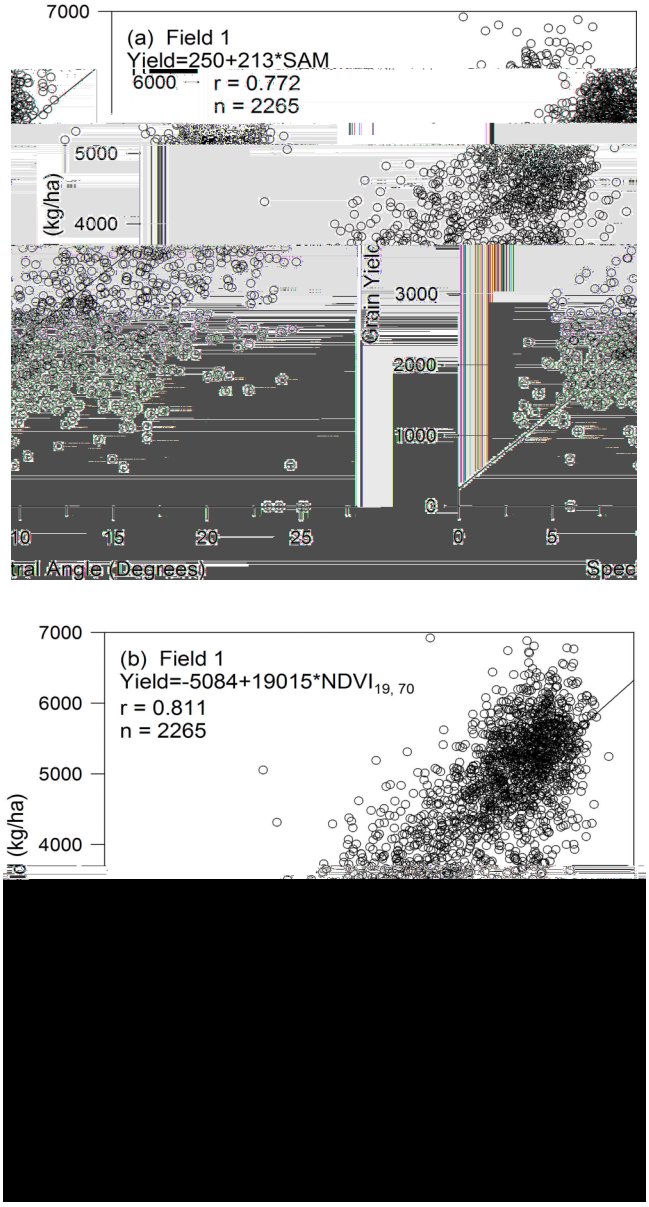

Figure 7. Scatter plot and regression line between grain sorghum yield monitor data and a SAM (spectral angle mapper) image derived from a 102-band airborne hyperspectral image for field 1 based on a dry soil reference spectrum extracted from the image, compared with the relationship between yield and the best narrow-band $NDVI_{19, 70}$ (band 19 = 543 nm and band 70 = 728 nm) for the field.

Summary and Conclusions

This study demonstrated the use of the SAM technique to derive SAM images from hyperspectral imagery for crop yield estimation. Six reference spectra extracted directly from the hyperspectral images and four reflectance spectra taken on the ground were used to derive SAM images. Statistical analysis showed that grain yield monitor data were significantly related to the SAM images. Although all the reference spectra produced similar correlation results, in practice it is more appropriate to use soil spectra for generating SAM images because soil spectra can be easily and accurately obtained.

Correlation analysis of yield with all 5151 possible NDVIs derived from the 102-band hyperspectral imagery indicated

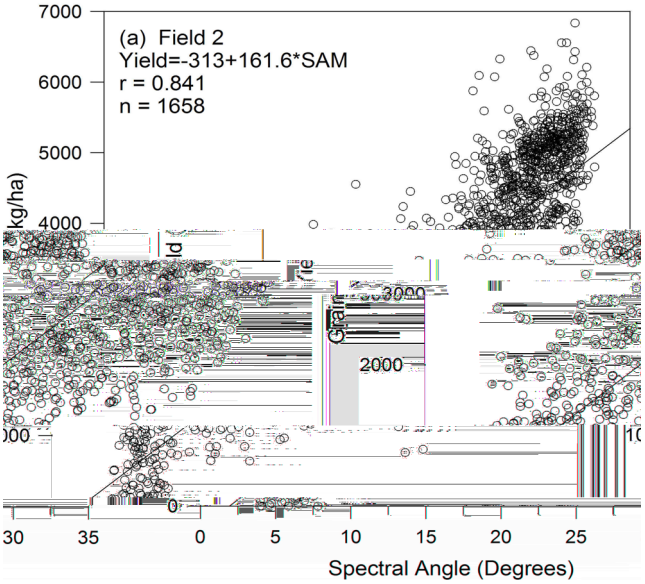

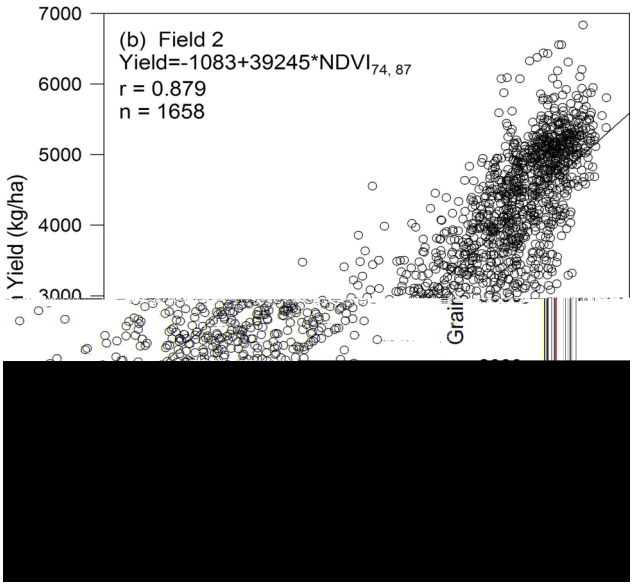

Figure 8. Scatter plot and regression line between grain sorghum yield monitor data and a SAM (spectral angle mapper) image derived from a 102-band airborne hyperspectral image for field 2 based on a dry soil reference spectrum extracted from the image, compared with the relationship between yield and the best narrow-band $NDVI_{74, 87}$ (band 74 = 742 nm and band 87 = 789 nm) for the field.

that although SAM images provided higher r-values than most of the NDVIs, the best NDVIs had better relations with yield. However, since each NDVI is based on only two narrow bands and a large number of NDVIs can be derived from a hyperspectral image, a single choice of two narrow bands could result in a poor representation of the yield variability. Generally, an NDVI calculated from a visible band and an NIR band can be a better representation than that derived from two visible bands or two NIR bands. Like an NDVI image, a SAM image can be easily generated from a hyperspectral image based on a soil reference spectrum to characterize the spatial variability in yield. In contrast, a SAM image uses all the spectral bands in the image, and can provide a reliable estimation of yield variability based on a single soil reference spectrum derived from the hyperspectral image or measured on the ground.

SAM provides researchers and practitioners an alternative or supplemental tool to reduce a hyperspectral image to a single-layer image for mapping yield variability. Like all VIs used in remote sensing, SAM has its own advantages and limitations. It can be used alone or in conjunction with other VIs for yield estimation. This study was the first to evaluate SAM for crop yield estimation, and more research is needed to evaluate this technique and explore its potential for deriving yield and other crop information.

Acknowledgements

We thank Rene Davis and Fred Gomez for acquiring the airborne hyperspectral imagery for this study and Jim Forward for assistance in image rectification. Thanks are also extended to Bruce Campbell and Rio Farms, Inc., Monte Alto, Texas, for use of their fields and harvest equipment.

References

Clark, M. L., D. A. Roberts, and D. B. Clark. 2005. Hyperspectral discrimination of tropical rain forest tree species at leaf to crown scales. *Remote Sensing Environ.* 96(3-4): 375-398.

Crósta, A. P., C. Sabine, and J. V. Taranik. 1998. Hydrothermal alteration mapping at Bodie, California, using AVIRIS hyperspectral data. *Remote Sensing Environ.* 65(3): 309-319.

Dennison, P. E., K. Q. Halligan, and D. A. Roberts. 2004. A comparison of error metrics and constraints for multiple endmember spectral mixture analysis and spectral angle mapper. *Remote Sensing Environ.* 93(3): 359-367.

Escobar, D. E., J. H. Everitt, J. R. Noriega, M. R. Davis, and I. Cavazos. 1997. A true digital imaging system for remote sensing applications. In *Proc. 16th Biennial Workshop on Color Photography and Videography in Resource Assessment*, 470-484. J. H. Everitt, ed., Bethesda, Md.: American Society for Photogrammetry and Remote Sensing.

Goel, P. K., S. O. Prasher, J. A. Landry, R. M. Patel, A. A. Viau, and J. R. Miller. 2003. Estimation of crop biophysical parameters through airborne and field hyperspectral remote sensing. *Trans. ASAE* 46(4): 1235-1246.

GopalaPillai, S., and L. Tian. 1999. In-field variability detection and spatial yield modeling for corn using digital aerial imaging. *Trans. ASAE* 42(6): 1911-1920.

Jang, G. S., K. A. Sudduth, S. Y. Hong, N. R. Kitchen, and H. L. Palm. 2005. Relating image-derived vegetation indices to crop yield. In *Proc. 20th Biennial Workshop on Aerial Photography, Videography, and High-Resolution Digital Imagery for Resource Assessment.* C. Yang and J. H. Everitt, eds., Bethesda, Md.: American Society for Photogrammetry and Remote Sensing.

Jordan, C. F. 1969. Derivation of leaf area index from quality of light on the forest floor. *Ecology* 50(4): 663-666.

Kruse, F. A., A. B. Lefkoff, J. W. Boardman, K. B. Heidebrecht, A. T. Shapiro, J. P. Barloon, and A. F. H. Goetz. 1993. The spectral image processing system (SIPS): Interactive visualization and analysis of imaging spectrometer data. *Remote Sensing Environ.* 44(2-3): 145-163.

Mundt, J. T., N. F. Glenn, K. T. Weber, T. S. Prather, L. W. Lass, and J. Pettingill. 2005. Discrimination of hoary cress and determination of its detection limits via hyperspectral image processing and accuracy assessment techniques. *Remote Sensing Environ.* 96(3-4): 509-517.

Plant, R. E., D. S. Munk, B. R. Roberts, R. L. Vargas, D. W. Rains, R. L. Travis, and R. B. Hutmacher. 2000. Relationships between remotely sensed reflectance data and cotton growth and yield. *Trans. ASAE* 43(3): 535-546.

Rouse, J. W., R. H. Haas, J. A. Shell, and D. W. Deering. 1973. Monitoring vegetation systems in the Great Plains with ERTS. In *Proc. 3rd ERTS Symposium*, 1: 309-317. NASA SP-351. Washington, D.C.: U.S. Government Printing Office.

Rowan, L. C., and J. C. Mars. 2003. Lithologic mapping in the Mountain Pass, California, area using Advanced Spaceborne Thermal Emission and Reflection Radiometer (ASTER) data. *Remote Sensing Environ.* 84(3): 350-366.

Senay, G. B., A. D. Ward, J. G. Lyon, N. R. Fausey, and S. E. Nokes. 1998. Manipulation of high spatial resolution aircraft remote sensing data for use in site-specific farming. *Trans. ASAE* 41(2): 489-495.

Thenkabail, P. S., R. B. Smith, and E. D. Pauw. 2000. Hyperspectral vegetation indices and their relationships with agricultural crop characteristics. *Remote Sensing Environ.* 71(2): 158-182.

Wiegand, C. L., A. J. Richardson, D. E. Escobar, and A. H. Gerbermann. 1991. Vegetation indices in crop assessments. *Remote Sensing Environ.* 35(2-3): 105-119.

Yang, C., and J. H. Everitt. 2002. Relationships between yield monitor data and airborne multispectral multidate digital imagery for grain sorghum. *Precision Agric.* 3(4): 373-388.

Yang, C., J. H. Everitt, and J. M. Bradford. 2002. Optimum time lag determination for yield monitoring with remotely sensed imagery. *Trans. ASAE* 45(6): 1737-1745.

Yang, C., J. H. Everitt, M. R. Davis, and C. Mao. 2003. A CCD camera-based hyperspectral imaging system for stationary and airborne applications. *Geocarto Intl. J.* 18(2): 71-80.

Yang, C., J. H. Everitt, and J. M. Bradford. 2004a. Airborne hyperspectral imagery and yield monitor data for estimating grain sorghum yield variability. *Trans. ASAE* 47(3): 915-924.

Yang, C., J. H. Everitt, J. M. Bradford, and D. Murden. 2004b. Airborne hyperspectral imagery and yield monitor data for mapping cotton yield variability. *Precision Agric.* 5(5): 445-461.